RSC Advances

PAPER

View Article Online
View Journal | View Issue

Cite this: *RSC Adv.*, 2019, **9**, 41877

An open-source programmable smart pipette for portable cell separation and counting†

Eunjung Lee,‡[a] Byeongyeon Kim‡[b] and Sungyoung Choi *[b]

Received 14th October 2019
Accepted 10th December 2019

DOI: 10.1039/c9ra08368e

rsc.li/rsc-advances

Microfluidics offers great potential for biomedical applications, but the complexity, inconvenience, and low pumping equipment accessibility of operating microfluidic devices have limited their widespread use. Here we describe an open-source, programmable smart (OS) pipette as an easy-to-use, simple, handheld microfluidic pump that overcomes the major limitations of previous commercial- or research-level pumps for microfluidics. The OS pipette pumps fluid into a microfluidic device by precisely controlling the position of the plunger of a positive-displacement micropipette with stepper motor control. The intuitive pumping mechanism of the OS pipette enables the novel features of simple fabrication, straightforward device operation, and precise, predictable, and programmable flow-rate generation as an open-source pumping tool. Controlling the OS pipette using an open-source microcontroller board not only allows straightforward generation of constant flow rates with simple source code commands, but also permits varying flow rates to be programmed (including stepwise increase and decrease of the flow rate over time, and flow-rate pulse generation). We successfully validate the OS pipette's capabilities for portable microfluidic cell separation and counting. The OS pipette has promise as a rapidly evolving and potentially transformative pumping tool that freely allows unrestricted use, distribution, reproduction, and modification even by non-expert users, and further enables diverse usages, even beyond microfluidics.

Introduction

Continuous and programmable flow-rate generation is important for the reliable operation of microfluidic devices, the performance of which often relies on flow conditions.[1–9] For example, most microfluidic cell separators and focusers have an optimum flow-rate range at which cells can have enough time to reach an equilibrium separation or focusing position by external forces[2–4] or intrinsic flow fields.[5–7] The signal intensity and counting sensitivity of microfluidic cell counters can vary significantly, depending on flow rates.[8,9] For such microfluidic applications, syringe pumps have been extensively used with high precision and smooth operation, despite bulky equipment size and high cost. In addition to commercially-available syringe pumps, a 3D-printed, open-source syringe pump has recently been developed,[10] creating low cost, highly customizable scientific equipment, and thus making available the essential fluidic equipment even for non-expert users to conduct microfluidic applications. However, even the open-source equivalent still employs the conventional operational process of filling a liquid sample into a syringe, and connecting tubing pieces between the syringe and a microfluidic device. Peristaltic pumps can be a versatile alternative to the syringe pumps,[11–13] easily creating recirculation systems, but they have definite limitations, such as intrinsic pulsation of peristaltic pumping, direct application of mechanical stresses to samples, and recurrent flow-rate calibrations. The development of microfluidics-compatible pumping methods with ease of use, high flow controllability, and stability is essential for the widespread use and commercialization of microfluidic technologies. Intensive efforts have been devoted to developing such pumping methods that can be categorized into passive and active approaches, depending on power usage.[14–26] Passive approaches can simply pump fluid samples without power consumption using pressure gradients generated by surface tension,[14] pressure head,[15,16] degassed gas-permeable materials,[17,18] absorbent,[19,20] capillary action,[21,22] pumping lid,[23] smart pipette,[24,25] and osmosis.[26] These passive principles are easy to use without the need for external equipment, and some of them can be embedded directly into microfluidic devices, thus resulting in the miniaturization of entire microfluidic systems. However, these methods often lack the ability to control the rate and direction of flow during pumping, and to generate high pressure flow conditions that can be essential for operating microfluidic devices that typically have high hydrodynamic resistance.

[a]*Department of Biomedical Engineering, Kyung Hee University, Yongin-si, Gyeonggi-do 17104, Republic of Korea*

[b]*Department of Biomedical Engineering, Hanyang University, Seoul 04763, Republic of Korea. E-mail: sungyoung@hanyang.ac.kr*

† Electronic supplementary information (ESI) available. See DOI: 10.1039/c9ra08368e

‡ E. Lee and B. Kim contributed equally to this work.

On the other hand, active approaches typically exhibit high fluidic controllability and are easy to generate high-pressure conditions, despite requiring external pumping and control equipment.[27–37] Peristaltic pumping mechanisms have been integrated into microfluidic devices by sequentially latching microfluidic pneumatic valves with high pressure sources and pneumatic controllers,[27,28] and by directly pressurizing elastomeric channels with Braille pins[29] or rotating magnets.[30] Electrokinetic pumps are suitable for fluid handling at micro- and nano-scales, and have been used for biomolecular separation.[31–34] Centrifugal pumping methods provide a simple and versatile way to pump, mix, and separate fluids on a spinning disk, and have been used to develop integrated microfluidic systems with a combination of on-disk filtration and sensing mechanisms.[35,36] Compared to the passive approaches, these active technologies can generate a wider range of flow rates, with a higher level of flow controllability. However, such methods often rely on bulky equipment to operate small microfluidic devices, or require the additional customization of existing microfluidic devices to fit into the pumping platforms. We previously developed a motorized smart pipette as a constant pressure generator to address the above technical challenges, by providing facile interconnection to general microfluidic devices, and similar usability to commercial micropipettes.[37] However, it is more appropriate for general microfluidic applications to pump fluids with constant flow rates rather than constant pressures, because it can obviate the need for recurrent flow-rate calibrations depending on fluid viscosity and channel resistance. Taken together, there is still an essential, but unmet need for a pumping tool that anyone can easily make and use for portable microfluidic applications.

Here, we present an open-source, simple, programmable smart (OS) pipette to pump fluid into a microfluidic device at highly precise, controllable rates that is as easy to use as commercial micropipettes. The OS pipette is engineered in an open-source format, by simply assembling commercially-available parts (*i.e.*, a stepper motor and a positive displacement pipette), and controlling it using an open-source microcontroller board. These unique features can freely allow potential users to access, use, and improve the hardware design and source code of the OS pipette. We explored the OS pipette's capabilities for precise and programmable flow-rate generation by directly comparing the fluid stream generated by the OS pipette and the fluid stream generated by a commercial syringe pump. We then demonstrated the ability of the OS pipette to translate microfluidic technologies into portable platforms for blood plasma separation and microflow cytometry applications. To the best of our knowledge, this is the first demonstration of a flow-rate generator for microfluidics in an open-source, portable, and programmable format. The OS pipette's portability, openness, ease of use, potential cost-effectiveness, and low system requirements for the operation of microfluidic devices will enable the widespread adoption of the devices, which have typically been limited to use in microfluidics research laboratories.

Materials and methods

Device fabrication

The OS pipette was fabricated simply by assembling commercially-available parts that included a stepper motor that contains a lead screw and a leadscrew nut (SL42STH40-1684A-300; Changzhou Fulling Motor Co., Ltd., China) ($21), a motor driver (A4988; Allegro MicroSystems, LLC, United States) ($0.8), a positive displacement pipette (Positive-Displacement Pipette MR-250; METTLER TOLEDO Corp., United States) ($410), a pipette tip (Prstrl 180/3 C-250; METTLER TOLEDO Corp., United States) ($0.4), aluminum posts (Custom-made product; Doo Kyoung Corp., Korea) ($30 each post) that had a setscrew with M3 threads in one end and a tapped hole for a M3 screw in the other, a 3D-printed holder ($4) that holds the motor and the pipette together, and a 3D-printed push block ($3) that converts the rotational motion of the motor into a linear motion, and transfers the mechanical force to the pipette plunger (Table S1 and Fig. S1†). The OS pipette was controlled using an Arduino Uno Rev3 main board (SparkFun Corp., United States) ($22).

A microfluidic comparator was fabricated by standard photolithography and polydimethylsiloxane (PDMS) replica molding, as reported elsewhere.[2–9] Briefly, the channel patterns of 57.5 μm height were photolithographically defined in a SU-8 photoresist film, and then transferred to PDMS by thermal curing of a mixture of PDMS and its curing agent at a 10 : 1 (wt/wt) mass ratio on the channel patterns. The final PDMS device has a single outlet and a 2 mm-wide junction channel connected to two inlet channels, allowing the direct comparison of the flow rates of two fluid streams injected into the device inlets.

The multi-layer SU-8 molds for a sheathless cell focuser and a blood plasma separator based on hydrophoresis were fabricated by two-step photolithography and PDMS replica molding, as described before.[38–41]The first and second layers of the sheathless focuser define a channel structure that gradually increases in width (21.6 μm in height) and ridge patterns (30.4 μm in height) formed on the channel structure, respectively. The first and second layers of the plasma separator define a channel network (13.2 μm in height) to connect separation channels in series and in parallel, and slant ridges (20.4 μm in height) formed on the channel network, respectively. After PDMS replica molding, all the PDMS devices were punched for inlet and outlet holes, and after air plasma treatment, irreversibly sealed with a glass slide. The OS pipette was either connected to the inlet of a PDMS device, or connected to the inlet *via* a PDMS adapter that was designed to fit its one end to the pipette tip, and the other end to a cut silicon tubing. Thus, the flexibility of the adapter can mitigate the effects of vibrational motion generated by the handheld use of the OS pipette on pumping.

A miniaturized fluorescence microscope was fabricated by simply assembling a laser diode (488 nm; DTR Laser, United States), a longpass filter with a cut-on wavelength of 515 nm (Omega Optical, Inc., United States), a 2× objective lens (Edmund Optics, Inc., United States), and a CMOS sensor (FLIR, Inc., Canada) in a 3D-printed housing, as described before.[9,21]

The field-of-view of the miniaturized microscope was 1.446 mm × 0.579 mm, which is large enough to capture the region of interrogation, the outlet channel region (400 μm in width) of the sheathless focuser.

All 3D printing design files used to make the smart pipette and the miniaturized microscope are provided in the ESI drawing.†

Sample preparation and analysis

A fluorescent dye (fluorescein) was purchased from Sigma-Aldrich Corp. (United States), dissolved in deionized water at a concentration of 10 μg mL^{-1}, and used to visualize the fluid stream pumped using the OS pipette. A bench-top fluorescence microscope (Nikon Corp., Japan) equipped with a high-speed camera (Vision Research, Inc., United States) was used to monitor the interfacial position between two fluid streams injected using the OS pipette and a commercial syringe pump (KD Scientific Inc., United States), and to measure fluorescent streaklines in the sheathless focuser. The OS pipette was used for all other experiments. Fluorescent polystyrene particles with a diameter of 15 μm were purchased from Thermo Fisher Scientific Corp. (United States), to demonstrate sheathless focusing and portable flow cytometry. Canine whole blood samples (a hematocrit level of 45%) were purchased from the Korea Animal Blood Bank (Korea) in compliance with safety regulations, for demonstration of blood plasma separation. The degree of hemolysis for centrifuged, sorted, and hemolyzed blood samples was determined by measuring the absorption of hemoglobin species in the wavelength range of 500 to 600 nm,[42] using a spectrophotometer (Eppendorf, Inc., Germany). We used a positive-displacement pipette with a maximum volume of 250 μL for the smart pipette assembly. The experiment time at the highest flow rate was less than 1 min so that there was no need to reload a sample solution. We also pre-wetted the pipette tip before connecting it to a microfluidic device, thereby preventing air bubbles from trapping in the device.

Smart pipette control and automatic image analysis algorithms

The speed of the stepper motor was controlled simply by setting a delay time (t_d) per revolution, as provided in the ESI.† For example, t_d was 100, 50, 25, 10, 5, 3.1, and 2.5 ms for the theoretical flow rates of 4.9, 9.7, 19.5, 48.7, 97.4, 155.8, and 194.8 μL min^{-1}, respectively. The interfacial position was measured 3.1 mm downstream from the point where the two fluid streams meet over time using a Matlab (MathWorks, Inc., United States) script. For the position measurement, the fluorescence intensity profiles were extracted from the corresponding pixel arrays in a fluorescence movie taken using a high-speed camera, and the length of the fluorescence region was calculated with a predefined scale. Automatic bead counting with a Matlab script was performed by sequentially analyzing fluorescence bead images taken using the miniaturized microscope. Fluorescence signals were continuously measured in the regions of interrogation, the outlet channel of the sheathless focuser with a width of 400 μm, and when the fluorescence level was larger than a threshold value, beads were identified and counted.

Numerical simulation

Numerical simulations were performed using COMSOL Multiphysics (https://www.comsol.com/comsol-multiphysics) to determine the nonlinear relationship between the interfacial position and the corresponding flow-rate ratio. A three dimensional finite element model was created in the same dimensions as the microfluidic comparator, and solved using the incompressible Navier–Stokes equation. The inlet boundary condition for one of the two inlets was varied from 1 to 160 μL min^{-1}, while the boundary condition for the other inlet was fixed at 20 μL min^{-1}. The outlet boundary condition was set to atmospheric pressure, and all other boundary conditions were set with no-slip boundary conditions. The interfacial position data for each flow rate condition were obtained by post-processing analysis, and a nonlinear relationship between the interfacial position and the corresponding flow-rate ratio was derived by fitting the simulation data with a power series model (Fig. S2†).

Results and discussion

Pumping principle and characterization

The OS pipette is based on the automatic position control of the plunger of a positive displacement pipette using a stepper motor (Fig. 1). The piston in the disposable pipette tip of the positive-displacement pipette makes direct contact with a sample fluid, allowing the pushing or pulling force of the plunger to be delivered directly to the piston or the fluid. Thus, at a given constant cross-section of the pipette tip, the OS pipette can produce precise, continuous, controlled flow rates, regardless of channel resistance and sample viscosity, simply by controlling the plunger position using the stepper motor. Synergistically combining a positive-displacement pipette and a stepper motor, which permits the simple two-step operational protocol of the OS pipette including (i) drawing up a sample fluid by releasing the plunger, and (ii) turning on the stepper motor, provides several significant advantages over previous pumping mechanisms for microfluidics (*e.g.*, syringe pumps and peristaltic pumps).

The first advantage is predictable, precise, continuous and calibration-free generation of the desired flow rates using the OS pipette. The volumetric flow rate of the OS pipette (Q_o) can be determined by multiplying the cross-sectional area of the pipette tip (A_{pt}) by the moving speed of the piston. Since the piston is directly controlled by the stepper motor, Q_o can be estimated by a specific incremental distance per step. The stepper motor contains a built-in lead screw and a traveling nut that convert a rotary motion to a linear motion, and directly transfer the mechanical force of the motor to the plunger, moving 8 mm per revolution (Fig. 1). Since the rotating speed of the motor is proportional to the input revolutions per minute (RPM) signals, the resulting Q_o can be controlled simply by RPM input, without any feedback mechanism. Thus, Q_o can be determined by $Q_o = A_{pt} \times D_s \times \mathrm{RPM}$, where D_s is the traveling

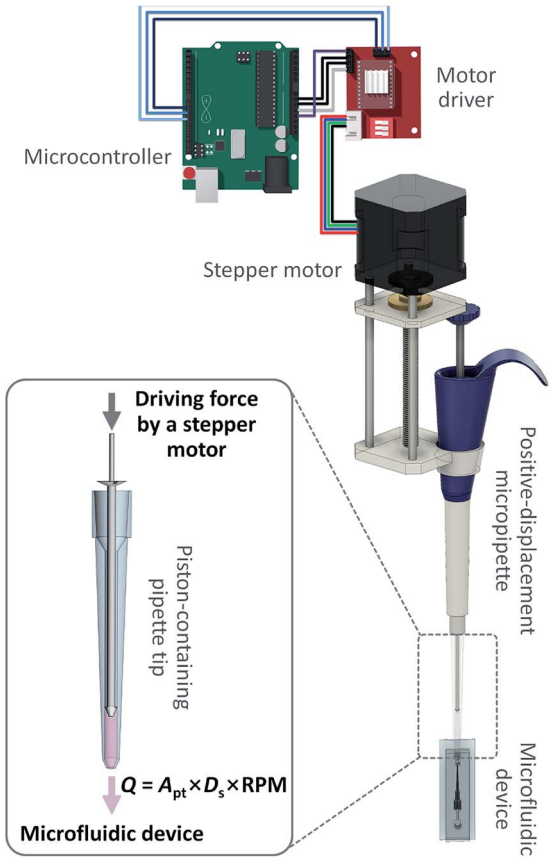

Fig. 1 Schematics of the OS pipette and its pumping principle. The OS pipette is a simple combination of a stepper motor and a positive-displacement pipette, which dispenses a sample fluid by directly moving the piston inside the pipette tip. Since the piston is in direct contact with the fluid, the mechanical force generated by the stepper motor can be transferred directly to the piston connected to the pipette plunger. This intuitive architecture enables precise generation of constant flow rates and time-varying flow rates through stepper motor control.

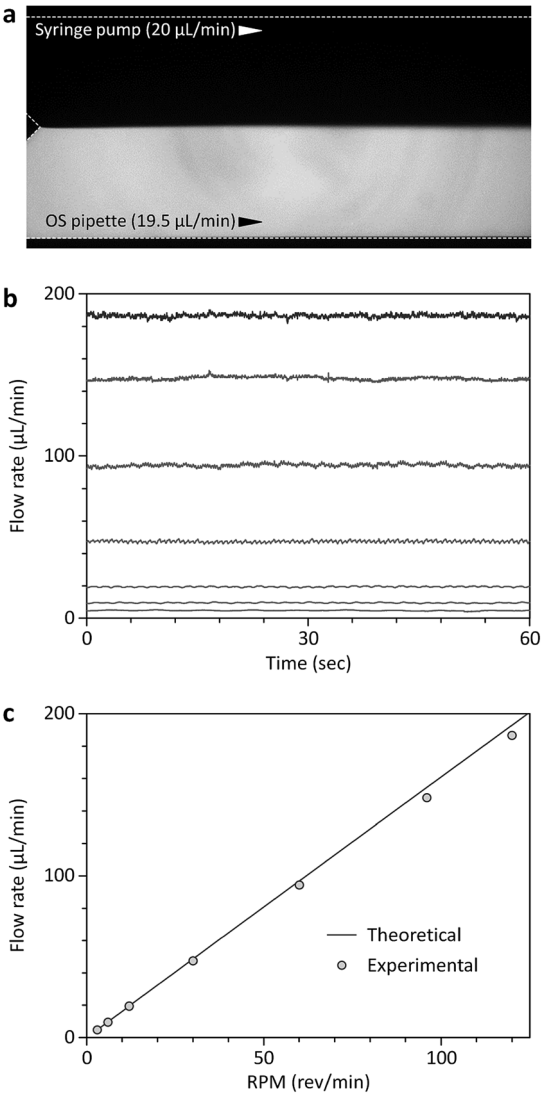

Fig. 2 Pumping performance of the OS pipette. (a) Fluorescence micrograph comparing two fluid streams pumped using the OS pipette and a commercial syringe pump. The interfacial positions measured over time were converted to the corresponding flow rate values through the flow rate-interfacial position relationship. (b) High pumping stability of the OS pipette with a CV of less than 4.3%. The set theoretical flow rates were 4.9, 9.7, 19.5, 48.7, 97.4, 155.8, and 194.8 μL min^{-1} from bottom to top. (c) Comparison of the experimental and theoretical flow rates for various RPM inputs ($n = 3$).

distance of the nut per revolution. We tested the pumping performance of the OS pipette in terms of pumping accuracy by comparing it with a commercial high-precision syringe pump (Fig. 2). For this comparative study, we used a well-characterized microfluidic comparator that allows direct comparison between the Q_o and the flow rate of the syringe pump (Q_s), by measuring the equilibrium interfacial position of the co-flowing, laminar streams of two fluids, and converting it to the Q_o relative to the Q_s (Fig. 2a). Fig. 2b and c show that the OS pipette could produce stable, continuous flows in a relatively wide range of flow rates from 4.8 to 186.7 μL min^{-1} with a coefficient of variation (CV) of less than 4.3% ($n = 3$). We note that the CV increased from 0.6 to 4.3% as the Q_o decreased from 186.7 to 4.8 μL min^{-1}, thereby impairing the pumping precision. This is attributed to the fact that the stepper motor converts electric pulses into discrete rotational step motions, and thus will not be smooth at low speeds, because the delay between step motions increases. However, this performance degradation can easily be improved by using lower volume positive-displacement pipettes and high-precision stepper motors, thus reducing the volume of fluid pumped per step. The theoretical and experimental Q_o results agree well with a relative error of less than 5.0% (Fig. 2c), demonstrating that the OS pipette allows predictable, precise, continuous and calibration-free generation of the desired flow rates.

The second advantage of the OS pipette is that it can provide a high degree of controllability for time-varying flow-rate control, which can be achieved through simple programming of an open-source microcontroller board. To test the dynamic characteristics of the OS pipette, we first measured its dynamic responses to step commands in the comparator by fixing the Q_s

to 20 μL min^{-1}, and abruptly increasing the Q_o from 19.5 μL min^{-1} to the desired flow rate (Fig. 3a and b). The settling time (t_s), which is defined as the time required for the response to become steady within 5% of a steady-state flow rate, took at least 1.2 s to reach the range of flow rates ≈38.8 to ≈95.9 μL min^{-1}. We then tested the pulse widths (w_p) that could reach the steady-state flow rate of 94.4 μL min^{-1} with $t_s = 1.2$ s. Fig. 3c and Movie S1† shows that the minimum w_p to reach the Q_o was 2 s, which was slightly larger than t_s, and below that, the steady-state flow rate could not be reached sufficiently, suggesting that t_s was an important parameter for the time-varying control of the OS pipette. Based on the characterized t_s, we successfully generated a horizontal step function that increased and decreased with a constant flow-rate step of ≈18 μL min^{-1} (Fig. 3d). These results demonstrate that the OS pipette provides the ability to control the relatively wide range of flow rates with a fast response time of less than 2.6 s, which can be implemented with simple Arduino source code commands provided in the ESI.†

The third advantage of the OS pipette is that it has the potential to change the stereotypes of the fabrication and use of high-precision pumps for microfluidics, while improving the accessibility and usability. The OS pipette was fabricated simply by assembling commercially-available parts (*i.e.*, a stepper motor, a positive-displacement pipette, and aluminum posts) and 3D-printed parts for holding the pipette, and pushing or pulling its plunger. This simple fabrication process will permit its unrestricted use, distribution, reproduction, and modification even by non-expert users, enabling its diverse usages, even for unexpected applications beyond microfluidics. In addition, unlike syringe pumps, which require filling a syringe with a sample fluid, removing air bubbles, connecting tubing pieces between the syringe and a microfluidic device, and loading the fluid into the devices, the OS pipette replaces these complex sample loading procedures with simple pipetting. Taken together, the OS pipette has a high degree of flow-rate controllability with the same ease of use as commercial motorized pipettes, and is straightforward to fabricate and modify, making it suitable for various microfluidic applications, as follows.

Microfluidic application 1: blood plasma separation. We applied the OS pipette to blood plasma separation, which is an important sample preparation step for liquid biopsy. Liquid biopsy is a promising technology for analysing molecular or cellular markers from a small volume of blood, and providing rapid feedback on patient condition.[43,44] Given the rapid degradation of blood *ex vivo*,[45,46] there is a critical need for rapid, on-site blood sample preparation. The portability of the OS pipette enables facile conversion of microfluidic plasma separators that depend on bulky, expensive syringe pumps to portable platforms when they are combined with the OS pipette.

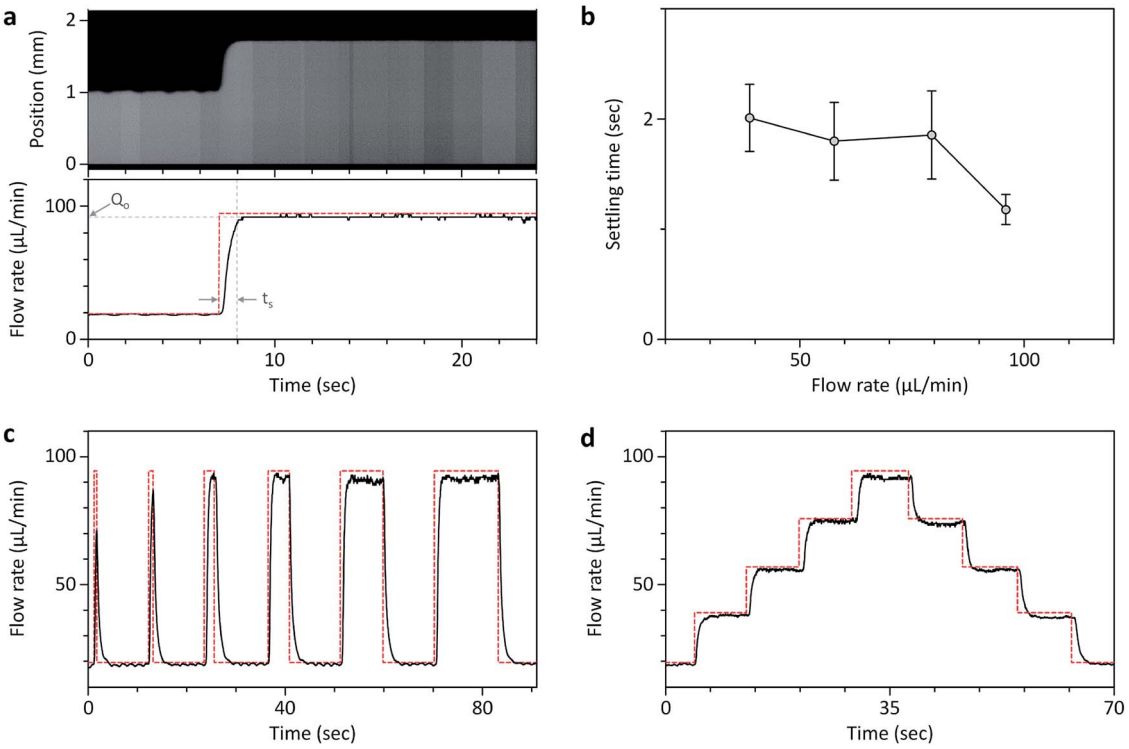

Fig. 3 Programmable pumping using the OS pipette. (a) Flow-rate response of the OS pipette (solid line) to a step command for a set flow rate of 94.4 μL min^{-1} (dotted line). The reconstructed fluorescence image shows the interfacial position measured 3.1 mm downstream from the point where the two fluid streams meet over time. (b) Settling time (t_s) according to the flow rate of the OS pipette (Q_o) ranged from 38.8 to 95.9 μL min^{-1} ($n = 3$). (c) Flow-rate response of the OS pipette (solid line) to pulse commands (dotted line). The set pulse widths were 0.5, 0.9, 2, 4, 8, and 12 s from left to right. (d) Flow-rate response of the OS pipette (solid line) to a profile of increasing and decreasing step commands with a set step of 18 μL min^{-1} (dotted line).

We tested the principle of continuous blood plasma separation based on grooved microchannels that has been developed by our group and others[40,41] as a model system. The separation principle is based on the lateral focusing of blood cells at an angle opposite to the inclination angle of the slant ridges, and the purity improvement by sequential drainage of focused blood cells and re-focusing of the remaining blood cells (Fig. 4).[40] Rotational flow streams induced by slant ridges direct blood cells to the sidewall, an equilibrium position, and steric interactions between the cells and the ridge structures prevent the cells from entering the ridges, while maintaining the focusing position. As operated using the OS pipette at an optimal flow rate of 186.7 μL min^{-1}, the plasma separator yielded high-purity blood plasma without hemolysis (Fig. 5 and Movie S2†). The plasma purity and recovery were 99.7 ± 0.1%

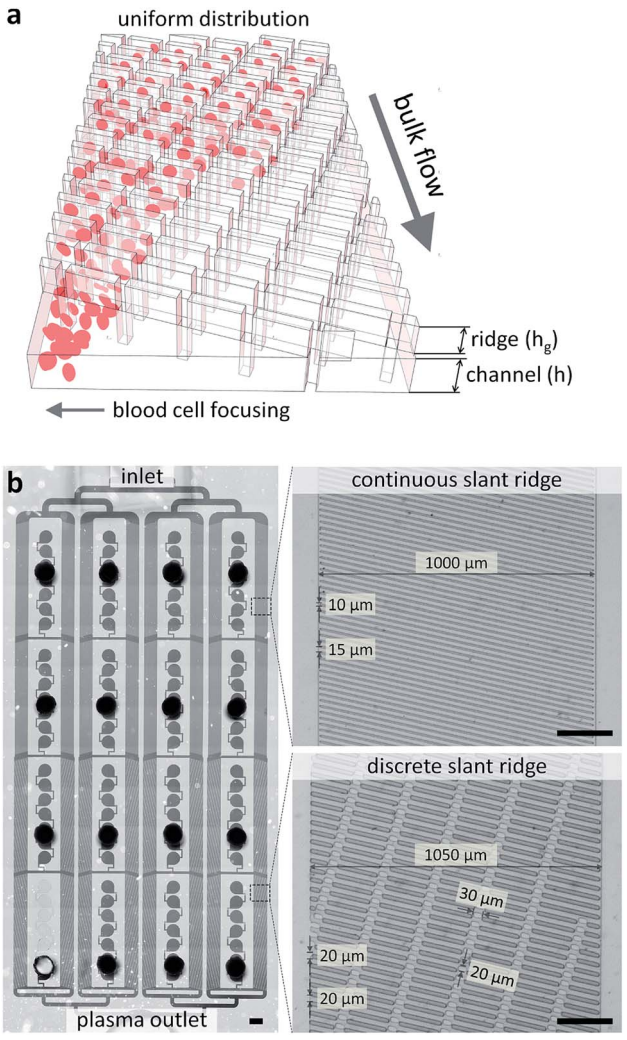

Fig. 4 Microfluidic blood plasma separator based on continuous slant array (CSA) and discrete slant array (DSA) ridges. (a) Based on ridge-induced rotational flows and collision-induced vertical displacement of blood cells, the cells can be focused at an angle opposite to the inclination angle of slant ridges. (b) The plasma separator consists of eight parallel separation units, each of which has two CSAs and two DSAs connected in series. Scale bar, 1 mm. The right panels show the enlarged views of the CSA and DSA ridges. Scale bar, 200 μm.

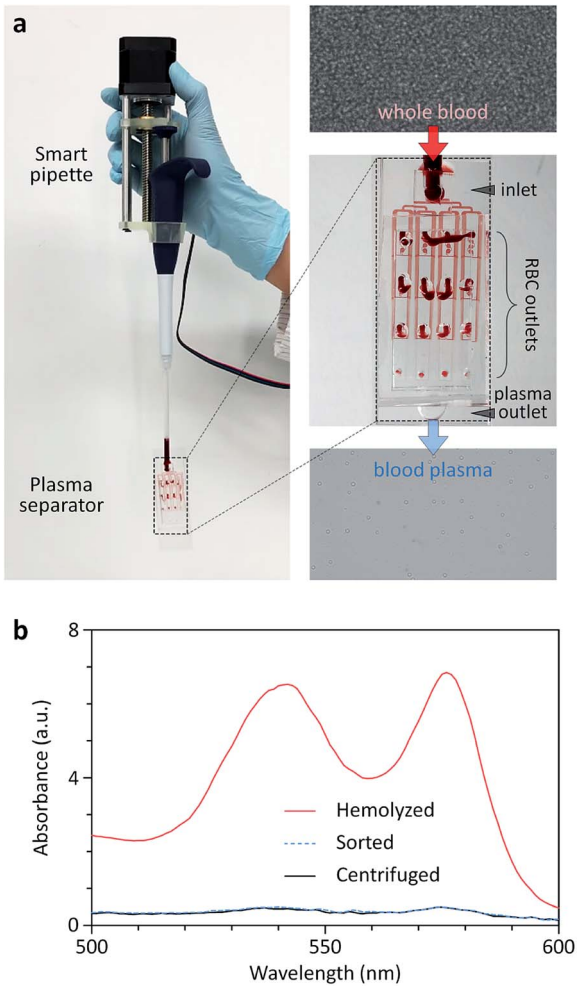

Fig. 5 Blood plasma separation using the OS pipette. (a) Handheld separation of blood plasma from whole blood using the microfluidic plasma separator and the OS pipette. (b) The blood plasma separation at 186.7 μL min^{-1} yielded high-purity blood plasma, removing 99.7% RBCs from whole blood. The absorption spectra of hemoglobin species for the hemolyzed, sorted, and centrifuged samples show hemolysis-free blood plasma separation by the slant array ridges. The oxyhemoglobin was released during the lysis of red blood cells.

and 20.6 ± 0.8%, which are defined as the ratio of the number of sorted blood cells in the sorted plasma to the initial whole number of blood cells, and the volume of plasma collected in the plasma outlet divided by the plasma volume of whole blood injected, respectively. These results collectively demonstrate that while fully implementing the functions of syringe pumps, the portable OS pipette can be used to operate microfluidic devices without additional modification and calibration, thus offering great promise in converting microfluidic technologies into portable platforms.

Microfluidic application 2: microflow cytometry. We next leveraged the ability of the OS pipette for portable and programmable flow-rate generation to make flow cytometry portable (Fig. 6 and 7). In addition to the portable pump, the OS pipette, we employed a hydrophoresis-based sheathless focuser to precisely deliver cells or particles without sheath fluid control

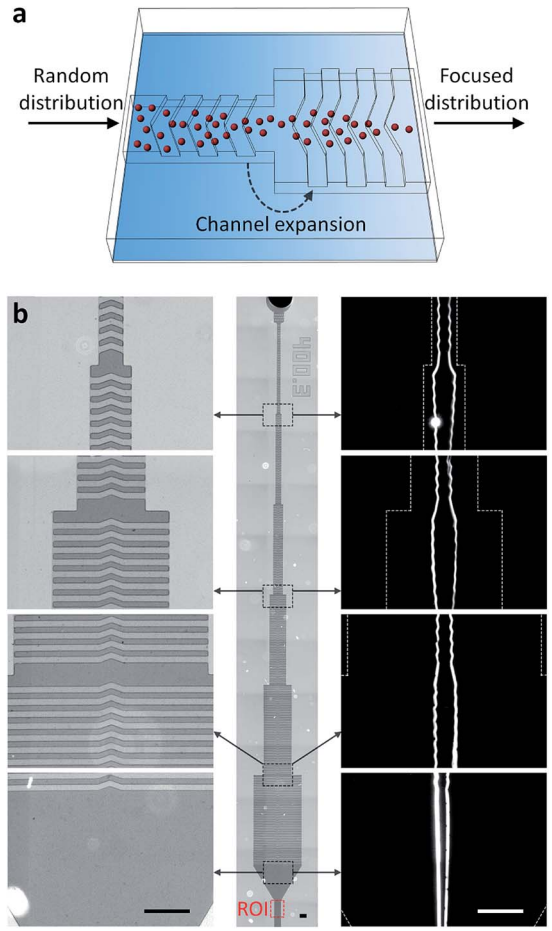

Fig. 6 Hydrophoresis-based sheathless cell focuser. (a) Microparticles can be guided by locally patterned, Λ-shaped ridges. Thus, as the channel width increases, the ratio of a particle focusing stream width to the channel width decreases, and the relative focusing efficiency improves. (b) Photographs of the sheathless focuser and fluorescence streakline images of 15 μm particles guided by the Λ-shaped ridges at a flow rate of 19.5 μL min^{-1}. Scale bars, 400 μm.

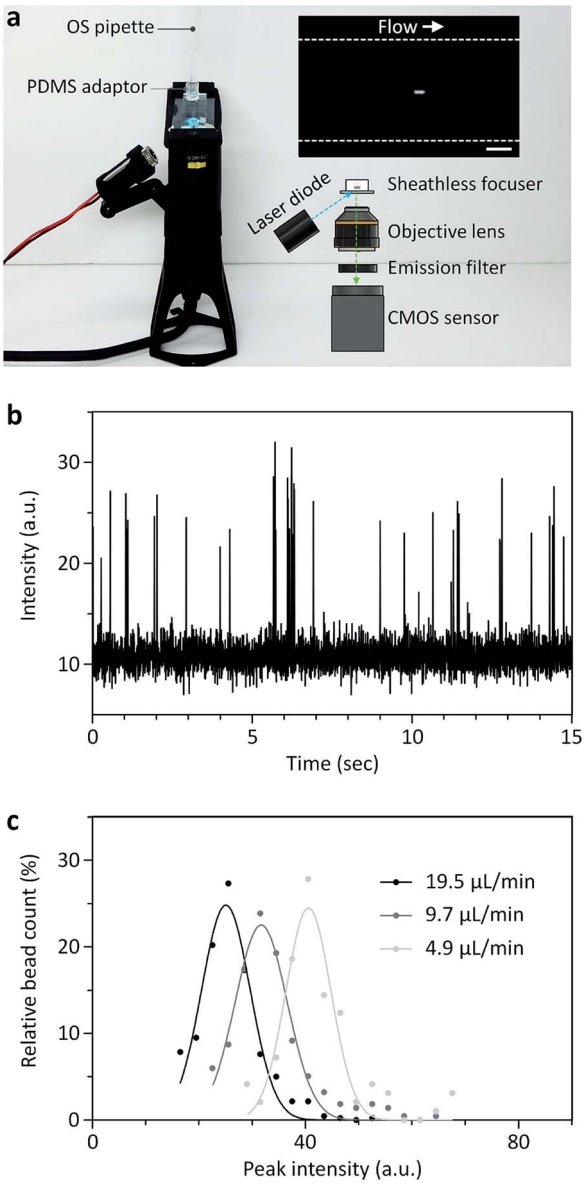

Fig. 7 Flow cytometric application of the OS pipette. (a) Photograph and schematic of the miniaturized fluorescence microscope for imaging flow cytometry that can capture the region of interrogation (ROI), the 400 μm-wide outlet region of the sheathless focuser. The top inset shows the snapshot of a 15 μm particle flowing through the ROI at a flow rate of 4.8 μL min^{-1}. Scale bar, 100 μm. (b) Fluorescence signals for 15 μm particles flowing at 19.5 μL min^{-1}. (c) Peak fluorescence-intensity histograms of 15 μm particles *versus* flow rate.

and external forces to a region of interrogation in a flow cytometer.[38,39] Thus, the fluidic system for flow cytometry can be greatly simplified, eliminating the need for bulky pumps, valves, and other auxiliary fluidic components, which has long been required for the operation of flow cytometry, and even microflow cytometry. In the channel configuration, particles can be guided by locally patterned, Λ-shaped ridges with a fixed width of 200 μm, while the channel width continues to widen from 0.2 to 2.8 mm (Fig. 6). Thus, as the channel expansion step increases, the focusing efficiency can be improved. Instead of bulky and expensive syringe pumps, we operated the sheathless focuser with the OS pipette, and measured the fluorescence intensity of the focused particles using the miniaturized microscope (Fig. 7). Double-stream focusing was achieved by injecting 15 μm fluorescent particles into the sheathless focuser at a flow rate of 19.5 μL min^{-1} using the OS pipette (Fig. 6b), which produced a uniform fluorescence peak intensity (I_{FL}) measured using the miniaturized microscope at 150 fps with a CV of less than 1.2% (Fig. 7). These results demonstrate that the OS pipette is capable of precise flow-rate generation, and is suitable for operating imaging flow cytometry, even though it is a hand-held type. We then tested the OS pipette to simulate the function of conventional flow cytometry that can tune the high-sensitivity mode at low speed, and the high-throughput mode at high speed. With the programmable pumping capability of the OS pipette, we increased Q_o from 4.8 to 19.5 μL min^{-1}. Fig. 7c shows that I_{FL} decreases with increasing Q_o while increasing the counting throughput from 68.3 to 323.5 particles per min. Thus, the OS pipette can enable flow-rate optimization either for

sensitive detection of dimly fluorescent particles, or high-throughput detection of a large population of cells. The counting throughput depends on the performance of the imaging sensor, which will be greatly improved by employing a high-speed, sensitive imaging sensor. Integrating multiple pipettes into the OS pipette can improve its versatility for more complicated microfluidic applications which require two or more different sample solutions (Fig. S3†). However, as the number of sample solutions increases, the size of the smart pipette will increase proportionally. Thus, further research on the pumping mechanism that can control multiple different solutions simultaneously with one pipette will be needed to improve the versatility of the smart pipette.

Conclusions

In summary, we developed an open-source, programmable smart pipette that enables portable operation of microfluidic devices while maintaining the functionalities of commercial syringe pumps. Compared to previous smart pipettes, a major improvement of the OS pipette is the synergetic combination of a stepper motor and a positive-displacement micropipette, thus enabling precise and programmable flow-rate generation. In addition, the fabrication method of simply assembling commercially-available components greatly increases the accessibility and availability of the OS pipette as an open-source platform, allowing its unrestricted use, distribution, reproduction, and modification, even by non-expert users. We demonstrated the utility of the OS pipette by converting microfluidic technologies for flow cytometry and blood plasma separation into portable platforms. The simple fabrication, ease-of-use, cost-effectiveness, and controllability of the OS pipette will make it a viable pumping tool for microfluidics in field-based and resource-limited settings. Based on the advantages we have demonstrated, the OS pipette can be extended to other microfluidic applications, or even to unexpected applications beyond microfluidics.

Conflicts of interest

There are no conflicts to declare.

Acknowledgements

This research was supported by Basic Science Research Program through the National Research Foundation of Korea (NRF) funded by the Ministry of Science, ICT & Future Planning (MSIP) (2019R1H1A1079944), and a NRF grant funded by the MSIP (2016R1A5A1010148).

References

1 C. K. Byun, K. Abi-Samra, Y.-K. Cho and S. Takayama, *Electrophoresis*, 2014, **35**, 245–257.
2 Y.-C. Kung, K.-W. Huang, W. Chong and P.-Y. Chiou, *Small*, 2016, **12**, 4343–4348.
3 J. Zhang, D. Yuan, Q. Zhao, S. Yan, S.-Y. Tang, S. H. Tan, J. Guo, H. Xia, N.-T. Nguyen and W. Li, *Sens. Actuators, B*, 2018, **267**, 14–25.
4 H.-S. Moon, K. Kwon, S.-I. Kim, H. Han, J. Sohn, S. Lee and H.-I. Jung, *Lab Chip*, 2011, **11**, 1118–1125.
5 Q. Zhao, J. Zhang, S. Yan, D. Yuan, H. Du, G. Alici and W. Li, *Sci. Rep.*, 2017, **7**, 41153.
6 A. J. Chung, D. R. Gossett and D. Di Carlo, *Small*, 2013, **9**, 685–690.
7 B. Kim, Y. J. Choi, H. Seo, E.-C. Shin and S. Choi, *Small*, 2016, **12**, 5159–5168.
8 D. M. Kalb, F. A. Fencl, T. A. Woods, A. Swanson, G. C. Maestas, J. J. Juarez, B. S. Edwards, A. P. Shreve and S. W. Graves, *Anal. Chem.*, 2017, **89**, 9967–9975.
9 B. Kim, S. Shin, Y. Lee, C. Um, D. You, H. Yun and S. Choi, *Sens. Actuators, B*, 2019, **283**, 549–555.
10 B. Wijnen, E. J. Hunt, G. C. Anzalone and J. M. Pearce, *PLoS One*, 2014, **9**, e107216.
11 P. Skafte-Pedersen, D. Sabourin, M. Dufva and D. Snakenborg, *Lab Chip*, 2009, **9**, 3003–3006.
12 X. Zhang, Z. Chen and Y. Huang, *Biomicrofluidics*, 2015, **9**, 014118.
13 W. Rhie and T. Higuchi, *J. Micromech. Microeng.*, 2010, **20**, 085036.
14 I. Meyvantsson, J. W. Warrick, S. Hayes, A. Skoien and D. J. Beebe, *Lab Chip*, 2008, **8**, 717–724.
15 X. Zhu, L. Y. Chu, B. Chueh, M. Shen, B. Hazarika, N. Phadke and S. Takayama, *Analyst*, 2004, **129**, 1026–1031.
16 K. Boonyaphon, Z. Li, G. Kim, C. S. Lim and S.-J. Kim, *Sens. Actuators, B*, 2018, **277**, 431–436.
17 L. Xu, H. Lee, D. Jetta and K. W. Oh, *Lab Chip*, 2015, **15**, 3962–3979.
18 S. Shin, B. Kim, Y.-J. Kim and S. Choi, *Biosens. Bioelectron.*, 2019, **133**, 169–176.
19 M. S. Sotoudegan, O. Mohd, F. S. Ligler and G. M. Walker, *Lab Chip*, 2019, **19**, 3787–3795.
20 Y.-C. Lee and W.-H. Hsieh, *Sens. Actuators, B*, 2014, **202**, 1078–1087.
21 B. Kim, S. Oh, S. Shin, S.-G. Yim, S. Y. Yang, Y. K. Hahn and S. Choi, *Anal. Chem.*, 2018, **90**, 8254–8260.
22 Y. Ye, Y. Zhao, J. Cheng, M. Li and C. Huang, *Micro Nano Lett.*, 2018, **13**, 1682–1687.
23 S. Begolo, D. V. Zhukov, D. A. Selck, L. Li and R. F. Ismagilov, *Lab Chip*, 2014, **14**, 4616–4628.
24 B. Kim and S. Choi, *Small*, 2016, **12**, 190–197.
25 B. Kim, Y. K. Hahn, D. You, S. Oh and S. Choi, *Analyst*, 2016, **141**, 5753–5758.
26 C. Xu, Y. K. C. Poh, I. Roes, E. D. O'Cearbhaill, M. E. Matthiesen, L. Mu, S. Y. Yang, D. Miranda-Nieves, D. Irimia and J. M. Karp, *PLoS One*, 2012, **7**, e44995.
27 M. C. Cole, A. V. Desai and P. J. A. Kenis, *Sens. Actuators, B*, 2011, **151**, 384–393.
28 T. Thorsen, S. J. Maerkl and S. R. Quake, *Science*, 2002, **298**, 580–584.
29 Y. S. Heo, L. M. Cabrera, J. W. Song, N. Futai, Y.-C. Tung, G. D. Smith and S. Takayama, *Anal. Chem.*, 2007, **79**, 1126–1134.

30 S.-Y. Tang, X. Zhang, S. Sun, D. Yuan, Q. Zhao, S. Yan, L. Deng, G. Yun, J. Zhang, S. Zhang and W. Li, *Adv. Funct. Mater.*, 2018, **28**, 1705484.
31 P. C. H. Li and D. J. Harrison, *Anal. Chem.*, 1997, **69**, 1564–1568.
32 L. Chen, H. Wang, J. Ma, C. Wang and Y. Guan, *Sens. Actuators, B*, 2005, **104**, 117–123.
33 L. Chen, S. Lee, J. Choo and E. K. Lee, *J. Micromech. Microeng.*, 2008, **18**, 013001.
34 Y. Li, Y. Ren, W. Liu, X. Chen, Y. Tao and H. Jiang, *Electrophoresis*, 2017, **38**, 983–995.
35 H.-K. Woo, V. Sunkara, J. Park, T.-H. Kim, J.-R. Han, C.-J. Kim, H.-I. Choi, Y.-K. Kim and Y.-K. Cho, *ACS Nano*, 2017, **11**, 1360–1370.
36 K. Sanger, K. Zór, C. B. Jendresen, A. Heiskanen, L. Amato, A. T. Nielsen and A. Boisen, *Sens. Actuators, B*, 2017, **253**, 999–1005.
37 B. Kim, D. You, Y.-J. Kim, I. Oh and S. Choi, *Sens. Actuators, B*, 2018, **267**, 581–588.
38 S. Song and S. Choi, *Cytometry, Part A*, 2013, **83**, 1034–1040.
39 S. Choi and J.-K. Park, *Anal. Chem.*, 2008, **80**, 3035–3039.
40 B. Kim, S. Oh, D. You and S. Choi, *Anal. Chem.*, 2017, **89**, 1439–1444.
41 S. Yan, J. Zhang, G. Alici, H. Du, Y. Zhu and W. Li, *Lab Chip*, 2014, **14**, 2993–3003.
42 W. G. Zijlstra and A. Buursma, *Comp. Biochem. Physiol., Part B: Biochem. Mol. Biol.*, 1997, **118**, 743–749.
43 R. Vaidyanathan, R. H. Soon, P. Zhang, K. Jiang and C. T. Lim, *Lab Chip*, 2019, **19**, 11–34.
44 Y. Sun, T. A. Haglund, A. J. Rogers, A. F. Ghanim and P. Sethu, *Anal. Chim. Acta*, 2018, **1012**, 10–29.
45 K. H. K. Wong, S. N. Tessier, D. T. Miyamoto, K. L. Miller, L. D. Bookstaver, T. R. Carey, C. J. Stannard, V. Thapar, E. C. Tai, K. D. Vo, E. S. Emmons, H. M. Pleskow, R. D. Sandlin, L. V. Sequist, D. T. Ting, D. A. Haber, S. Maheswaran, S. L. Stott and M. Toner, *Nat. Commun.*, 2017, **8**, 1733.
46 L.-H. Huang, P.-H. Lin, K.-W. Tsai, L.-J. Wang, Y.-H. Huang, H.-C. Kuo and S.-C. Li, *PLoS One*, 2017, **12**, e0184692.